SF2A 2008
C. Charbonnel, F. Combes and R. Samadi (eds)

HIGH-RESOLUTION THERMAL IR IMAGING OF MWC300 WITH VLT/VISIR

Domiciano de Souza, A.[1], Kervella, P.[2], Bendjoya, Ph.[1] and Niccolini, G.[1]

Abstract. B[e] stars are expected to possess dusty circumstellar environments, which are responsible for a strong infrared (IR) excess. Using single-dish diffraction-limited imaging in the thermal infrared domain, we aim at measuring the angular extension of the dusty environment of the galactic B[e] MWC 300. We obtained diffraction-limited images of MWC 300 at 11.25 μm using the BURST mode of the VLT/VISIR instrument. MWC 300 is partially, but statistically significantly, resolved by VISIR so that we could measure the size of its dusty envelope for the first time. By assuming a 2D circular Gaussian intensity distribution and using different image analysis methods we measured a FWHM angular size of 69 ± 10 mas. For a distance of 1.8 kpc, we obtain a linear size of 125 ± 18 AU = $(1.87 \pm 0.26) \times 10^{13}$ m for the circumstellar dust emitting in the mid-IR. This measured size is shown to agree with a model that was calculated with a Monte Carlo radiative transfer code for dust envelopes. The flux of MWC 300 at 11.25 μm is estimated as 84.5 ± 1.4 Jy = $(20.0 \pm 0.3) \times 10^{-13}$ W/m^2/μm. The VLT/VISIR now offers the possibility of obtaining mid-IR diffraction-limited images with a high signal-to-noise ratio. The MWC 300's size as directly measured in this work is compatible with the theoretical size of a nearly edge-on dusty disc estimated in previous works. Interferometric data at milliarcsec angular resolution are required to reveal details on this dusty envelope.

1 Introduction

MWC 300 (V431 Sct) is a galactic B[e] star, being most probably a supergiant B[e] with a luminosity $\log L/L_{\odot} = 5.1 \pm 0.1$ and located at a distance $d = 1.8 \pm 0.2$ kpc (Miroshnichenko et al. 2004; hereafter M04). Interferometric and/or imaging instruments can nowadays attain the required angular resolutions for directly measuring the mid-IR size of MWC 300 and of other supergiant B[e] stars (e.g., Domiciano de Souza et al. 2007).

We present here results from diffraction-limited images of MWC 300 at 11.25 μm using the BURST mode of the VLT/VISIR instrument. This work is based on observations performed at the European Southern Observatory, Chile under ESO Program 078.D-0295(A). A detailed description of the results is given by Domiciano de Souza et al. (2008).

2 Observations and data reduction

We used the VISIR instrument (Lagage et al. 2004), installed at the Cassegrain focus of the Melipal telescope (UT3) of the VLT (Paranal, Chile). Under standard conditions at Paranal (median seeing of 0.8" at 0.5 μm), the 8 m telescope is not diffraction-limited in the mid-IR (seeing ≈ 0.4" vs. 0.3" diffraction).

To overcome this limitation, a specific mode of the instrument called the BURST mode was introduced by Doucet et al. (2007). Its principle is to acquire very short exposures ($\Delta t \leq 50$ ms), to keep the complete integration within a fraction of the coherence time (≈ 300 ms at Paranal in the mid-IR). The detector is therefore read very quickly, and the resulting images freeze the turbulence. It is subsequently possible to select the best images presenting a single speckle ("lucky imaging"), so they are diffraction-limited.

We observed MWC 300 during the first half of the night of October 3-4, 2006. A series of BURST mode observations of this star and its main PSF calibrator η Ser (HD 168723, spectral type K0III-IV) was obtained in the PAH2 filter, whose central wavelength is $\lambda = 11.25$ μm. The main PSF calibrator, η Ser, was chosen in the Cohen et al. (1999) catalogue of spectrophotometric standards for infrared wavelengths so that its flux is

[1] Lab. H. Fizeau, CNRS UMR 6525, Univ. de Nice-Sophia Antipolis, Observatoire de la Côte d'Azur, F-06108 Nice cedex 2
[2] LESIA, Observatoire de Paris, CNRS UMR 8109, UPMC, Université Paris Diderot, 5 Place Jules Janssen, F-92195 Meudon

Table 1. Log of the VISIR observations of MWC 300 and its main (PSF1: η Ser) and secondary (PSF2: α Eri) PSF calibrators.

#	MJD[1]	Star	DIT[2]	N exp.[3]	θ (")[4]	AM[5]
img A	0.0044	MWC 300	10	1200 × 8	0.8	1.15
img B	0.0120	MWC 300	10	1200 × 14	1.1	1.21
img C	0.0238	MWC 300	10	1200 × 14	1.0	1.24
PSF1	0.0451	η Ser	10	1200 × 14	1.0	1.46
PSF2	0.1877	α Eri	20	1200 × 14	0.8	1.21

[1] modified Julian date of the middle of the exposures on the target, minus 54 012.

[2] Detector Integration Time given in milliseconds for one frame.

[3] number of image exposures in the form *nb. of frames per file* × *nb. of files.*

[4] seeing in the visible ($\lambda = 0.5\,\mu$m) as measured by the observatory DIMM sensor, in arcseconds.

[5] average airmass of the observation.

absolutely calibrated, providing a convenient photometric reference for accurately estimating the absolute flux of MWC 300. We estimated the flux of MWC 300 at 11.25 μm to be 84.5 ± 1.4 Jy = $(20.0 \pm 0.3) \times 10^{-13}$ W/m^2/μm. This value is in good agreement with other measured fluxes in the mid-IR: for example M04 found 76.5 Jy at 10.79 μm, and the MSX observations give 70.0 Jy at 8.28 μm and 93.6 Jy at 12.13 μm (Egan et al. 2003). A secondary PSF (PSF2: α Eri) has also been used in the data analysis.

The journal of the VISIR observations is given in Table 1. During the observations, the seeing quality in the visible varied from 0.8 to 1.1".

2.1 Raw data processing

The fluctuations of the thermal background were removed through the classical subtraction of the chopped and nodded images, to produce data cubes of about 10 000 images covering 6.8" × 6.8". After a precentering at the integer pixel level, the images were sorted by their maximum intensity, used as a proxy of the Strehl ratio (e.g., Born & Wolf 1999). The 40% best images of each cube were then resampled up by a factor 10 using a cubic spline interpolation, and the star image was subsequently centered using Gaussian fitting, at a precision level of a few milli arc seconds (much smaller than the original pixel scale). The field of view was trimmed to 2.25" × 2.25" to reduce the computing time. The resulting cubes were eventually averaged to obtain the master images of MWC 300 and the PSFs used in our image analysis.

The final averaged images of MWC 300 and η Ser are shown in Fig. 1. We can see up to 3 or 4 Airy rings in all MWC 300 images. We note that the data signal-to-noise ratio (SNR) is quite high, reaching $\simeq 2500 - 3500$ per pixel in the core of the MWC 300 images; for the PSF1 the SNR reaches $\simeq 1900$ per pixel. Thanks to these high SNRs one can determine that the core of the MWC 300 images are statistically significantly wider than the core of the PSF, suggesting that the target was partially resolved by VISIR.

3 Image analysis

We applied different methods to estimate MWC 300's size at 11.25 μm from the partially resolved VISIR images:

1. Size estimation assuming that the central peaks of all images (MWC 300 and PSFs) can be represented by a 2D circular Gaussian (hereafter 2DCG).

2. Size estimation by fitting the MWC 300 images with a 2DCG convolved with the observed PSF image. Here we assume that the real intensity distribution of MWC 300 is given by a 2DCG profile.

3. Size estimation by direct image deconvolution of the MWC 300 images by the PSFs. The only assumption about MWC 300 adopted for the deconvolution is that it has a positive intensity distribution, i.e., the positivity criterion commonly used in image processing.

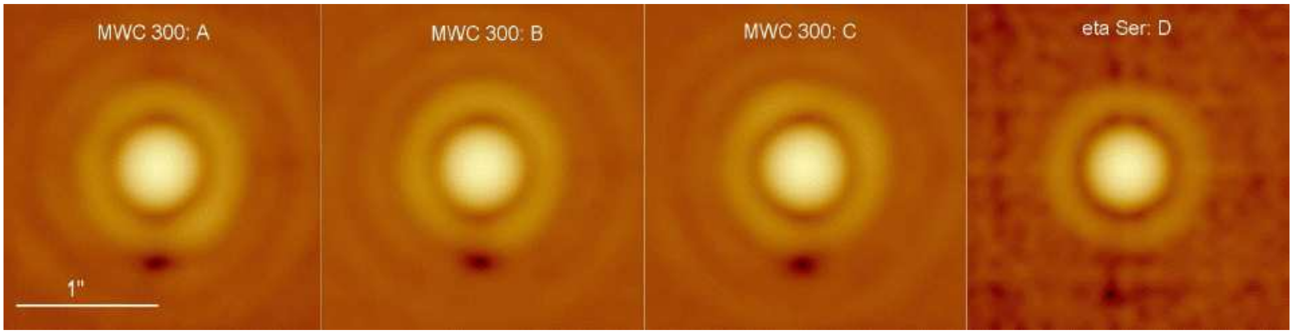

Fig. 1. Final averaged images of MWC 300 and η Ser (PSF) in logarithmic scale (see text and Table 1 details about the observations). At least 3 Airy rings are visible in MWC 300.

Table 2. Typical size of MWC 300 (2D circular Gaussian FWHM in units of mas) from different methods for the VISIR images A, B, and C.

Method applied:	A	B	C	$\overline{\mathrm{FWHM}} \pm \sigma$
Analytical estimation	70	62	57	63 ± 7
Fit of 2DCG convolved with PSF	81	72	67	73 ± 7
Richardson-Lucy deconvolution	80	68	60	69 ± 10

The main results are summarized in Table 2 and the details of each method used are given by Domiciano de Souza et al. (2008). In the following we describe the results from the decovonlution method, which is the one imposing less *a priori* constraints on the data.

3.1 Imaging by Richardson-Lucy deconvolution

We thus performed a Richardson-Lucy deconvolution using the software package Airy[1] (Correia et al. 2002) version 4.0, developed within the CAOS problem-solving environment. The size of the deconvolved images diminishes regularly at each iteration, reaching a plateau after a few hundred iterations. To estimate the size of the deconvolved images and more easily compare it with the sizes from the other methods, we fitted a 2DCG to measure the corresponding FWHM after each iteration. Figure 2(left) shows the FWHM of the MWC 300 deconvolved images as function of the deconvolution iteration.

The deconvolution process was repeated until 1000 iterations to make sure that the FWHM of the deconvolved images converged to a minimum or a plateau in our case. We present in Table 2 the average FWHM calculated on the central peak of the deconvolved images at the plateau regime. This plateau regime is considered to have been reached when the FWHM varies by less than 0.2% between two iterations. The final results do not strongly depend on this value.

The sizes obtained from deconvolution are compatible with the first two methods, especially with those from the fit of a 2DCG convolved with the PSF. As an example of a deconvolved image, we also show in Fig. 2(left) the average of images A, B, and C of MWC 300 deconvolved by the PSF1 at iteration 1000. The more intense secondary structures in the deconvolved image are residuals from the first Airy ring, probably caused by the fact that the SNR of the MWC 300 images is larger than for the PSF.

Since the deconvolution does not impose any a priori assumption on MWC 300, we chose the average size and uncertainty from this method as the more realistic size estimation from the VISIR data: FWHM $= 69 \pm 10$ mas. From our angular size estimation (FWHM $= 69 \pm 10$ mas from the deconvolution), the linear FWHM of MWC 300 at 11.25 μm is $\mathrm{FWHM}_{\mathrm{linear}} = 125 \pm 18$ AU $= (1.87 \pm 0.26) \times 10^{13}$ m (assuming a distance $d = 1.8$ kpc given by M04). For a central star radius $R_* = 29\ R_\odot$, from M04, we have $\mathrm{FWHM}_{\mathrm{linear}} = 924 \pm 131 R_*$.

[1]available at http://fizeau.unice.fr/caos/

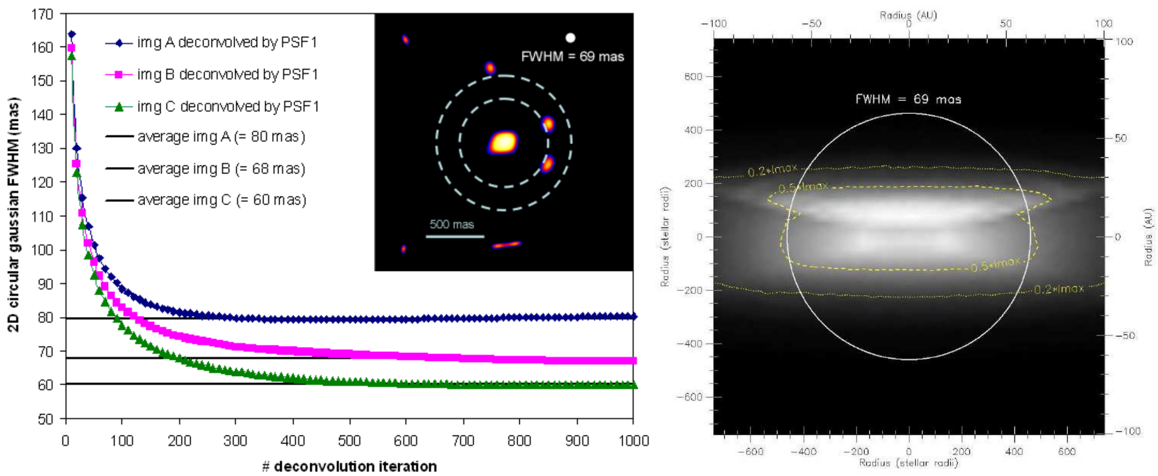

Fig. 2. *Left:* FWHM from a fit of a 2DCG to the center of each deconvolved image of MWC 300 as a function of the iteration number. After a few hundred iterations, the MWC 300 deconvolved images converge to an almost constant FWHM. The average FWHM of each MWC 300 deconvolved image calculated on the plateau regime is compatible with the estimations from other methods (Table 2). The upper right image shows the average of images A, B, and C deconvolved by the PSF1 at iteration 1000 (log. scale). The dashed rings indicate the first Airy ring region. The 2DCG FWHM from the deconvolution method is indicated. *Right:* Image of MWC 300 calculated with a Monte Carlo radiative transfer code (Niccolini & Alcolea 2006). This 11.25 μm image corresponds to a nearly equator-on disc (inclination of the polar axis to the line of sight is 80°). Note that the size of the image at half intensity (dashed contour) agrees with the FWHM size measured with VISIR (circle).

4 Modelling by Monte Carlo radiatif transfer

For a more quantitative analysis of our size estimation, we computed a model dusty disc with the help of a Monte Carlo continuum radiative transfer code (Niccolini & Alcolea 2006). The model input parameters are those of M04, except for the mass of the disc ($M = 0.01 M_\odot$) and for the density profile, which in our case is given by a Gaussian law from $R_1 = 147 R_*$ to $3450 R_*$, followed by a $\rho \propto r^{-4}$ power-law. The synthetic image at 11.25 μm, shown in Fig. 2(right), well agrees with the measured VISIR FWHM. The adopted model gives dust temperatures above ~ 600 K within the measured FWHM.

References

Born, M. & Wolf, E. 1999 Principles of Optics, 7th ed. Cambridge, England: Cambridge University Press

Cohen, M., Walker, R. G., Carter, B., et al. 1999, AJ, 117, 1864

Correia, S., Carbillet, M., Boccacci, P., et al. 2002, A&A, 387, 733

Domiciano de Souza, A., Kervella, P., Bendjoya, P., & Niccolini, G. 2008, A&A, 480, L29

Domiciano de Souza, A., Driebe, T., Chesneau, O., et al. 2007, A&A, 464, 81

Doucet, C., Habart, E., Pantin, E. et al. 2007, A&A, 470, 625

Egan, M.P., Price, S.D., Kraemer K.E., et al. 2003, The Midcourse Space Experiment Point Source Catalog Version 2.3, AFRL-VS-TR-2003-1589

Lagage, P.O. et al. 2004, The ESO Messenger 117, 12

Miroshnichenko, A. S., Levato, H., Bjorkman, K. S. et al. 2004, A&A, 417, 731

Niccolini, G., & Alcolea, J. 2006, A&A, 456, 1